

ENCLOSURE 2

MFN 07-478

NEDO-33173, Supplement 1

Non-Proprietary Version

IMPORTANT NOTICE

This is a non-proprietary version of Enclosure 1 to MFN 07-478, NEDC-33173P, Supplement 1, which has the proprietary information removed. Portions of the enclosure that have been removed are indicated by an open and closed bracket as shown here [[]]

GE-Hitachi Nuclear Energy Americas, LLC

3901 Castle Hayne Rd
Wilmington, NC 28401

NEDO-33173, Supplement 1

Revision 0

Class I

eDRF Section 0000-0060-5204-01

August 2007

NON-PROPRIETARY VERSION

Licensing Topical Report

**VOID FRACTION ERROR BASED ON 10X10 FUEL PRESSURE
DROP DATA**

Legal Notice

The document contains proprietary information of GE-Hitachi Nuclear Energy Americas, LLC (GEH) and is furnished in confidence for the purpose(s) stated in the transmittal letter. No other use, direct or indirect, of the document or the information it contains is authorized. Furnishing this document does not convey any license, expressed or implied, to use any patented invention. The recipient shall not publish or otherwise disclose this document or the information therein to others without prior written permission of GEH.

Neither GEH nor any of the contributors to this document makes any warranty or representation (expressed or implied) with respect to the accuracy, completeness, or usefulness of the information contained in this document; or that the use of such information may not infringe privately owned rights; nor do they assume any responsibility for liability or damage of any kind which may result from the use of any of the information contained in this document.

Non-Proprietary Notice

This is a non-proprietary version of the document NEDC-33173P, Supplement 1, which has the proprietary information removed. Portions of the document that have been removed are indicated by open and closed double brackets as shown here [[]].

Copyright, GE-Hitachi (GEH), 2007

TABLE OF CONTENTS

1.0	INTRODUCTION, SCOPE, AND OBJECTIVE.....	1-1
2.0	ASSUMPTIONS.....	2-1
3.0	APPROACH AND METHODS.....	3-1
4.0	ANALYSIS AND RESULTS.....	4-1
4.1	PREDICTED VERSUS MEASURED ΔP	4-1
4.2	PRESSURE DROP BIAS AND UNCERTAINTY.....	4-3
4.3	CALCULATED STEADY STATE VOID FRACTION BIAS	4-4
4.4	VOID FRACTION UNCERTAINTY TREATMENT.....	4-6
4.4.1	<i>Approach</i>	4-6
4.4.2	<i>Void and ΔP Relationship</i>	4-7
4.4.3	<i>Measurement Uncertainties in the ΔP Experiments</i>	4-7
4.5	VOID ERROR ESTIMATE	4-8
4.5.1	<i>Void Fraction Bias and Uncertainty Based on GE14 Data</i>	4-8
4.5.2	<i>Void Fraction Bias and Uncertainty Based on GNF2 Data</i>	4-9
4.6	COMPARISON TO THE FINDLAY-DIX CORRELATION DATABASE.....	4-11
5.0	EVALUATION, SUMMARY, AND CONCLUSIONS	5-1
5.1	GENERAL	5-1
5.2	IMPACT OF KEY ASSUMPTIONS ON CONCLUSIONS	5-1
5.2.1	<i>Trend Analysis</i>	5-3
5.2.2	<i>Correlation Analysis</i>	5-5
5.3	INTEGRAL VERSUS LOCAL ERRORS.....	5-8
5.4	CONFIRMATORY LOW FLOW DATA SUBSETS	5-10
5.5	SUMMARY	5-14
	APPENDIX A. 1-D FLOW QUALITY, EQUILIBRIUM QUALITY, AND VOID FRACTION	A-1
A.1.	QUALITY	A-1
A.2.	VOID FRACTION	A-2
A.2.1.	<i>Example Based on GNF2 Data</i>	A-3
A.2.2.	<i>Example Based on GE14 Data</i>	A-4
A.3.	APPLICATION TO REACTOR SIMULATION	A-5
A.3.1.	<i>Expected Void Fraction Ranges for Peak Bundles</i>	A-6
A.3.2.	<i>Planar Average Versus Local (Subchannel) Void Fractions</i>	A-8
	APPENDIX B. "METHOD B" PRESSURE DROP	B-1
	APPENDIX C. ATLAS MEASUREMENT UNCERTAINTIES	C-1

TABLE OF CONTENTS

REFERENCES R-1

LIST OF FIGURES

Figure 4-1.	GE14 Pressure Drop Comparisons	4-1
Figure 4-2.	GNF2 Pressure Drop Comparisons.....	4-2
Figure 4-3.	GE14 Pressure Drop Statistics	4-8
Figure 4-4.	GNF2 Pressure Drop Statistics	4-10
Figure 5-1.	Calculated Elevation ΔP Versus Void Fraction Based on Equation (4.9)	5-3
Figure 5-2.	GE14 ΔP Data Predicted with Method B [1].....	5-4
Figure 5-3.	GNF2 ΔP Data Predicted with Method B.....	5-5
Figure 5-4.	Pressure Drop Error (δP) Versus Power-to-Flow Ratio	5-6
Figure 5-5.	Pressure Drop Error (δP) Versus Mass Flux.....	5-7
Figure 5-6.	GNF2 ΔP (Calculated or Measured) Versus Elevation.....	5-8
Figure 5-7.	GNF2 ΔP (Calculated or Measured) Versus Elevation for Low Flow Rate Test Runs.....	5-9
Figure 5-8.	GE14 ΔP (Calculated or Measured) Versus Mass Flux for the 0 to 3 MWt Test Runs.....	5-10
Figure A-1.	Generic $MCPR_F$	A-6
Figure A-2.	Predicted Exit Void Fractions Based on Critical Power Data.....	A-7

LIST OF TABLES

Table 4-1.	Predicted Versus Measured Data Summary – Spacer ΔP Tests [1].....	4-2
Table 4-2.	Multi-Rod Experimental Data Used to Validate The Findlay-Dix Correlation.....	4-11
Table 5-1.	Low Flow Rate ΔP Test Summary [1].....	5-11
Table 5-2.	Low Flow Rate Calculated Void Bias and Standard Deviation.....	5-12
Table 5-3.	Low Flow Rate Data Test Comparisons	5-13
Table B-1.	Expressions Applied to Calculate the In-Channel Pressure Drop.....	B-1
Table C-1.	Measurement Uncertainties [2]	C-1

NEDO-33173, Supplement 1
Non-proprietary Version

Abstract

This document provides the results of an analysis to evaluate the accuracy of the Findlay-Dix void correlation as applied to GNF 10x10 fuel designs. The analysis is based on steady state pressure drop measurements taken from full-scale thermal-hydraulic tests. Relating pressure drop errors to errors in calculated void fraction provides a quantitative basis for evaluation. The results of this analysis indicate that there is no evidence that the accuracy of Findlay-Dix is degraded relative to its original validation basis when applied to contemporary 10x10 fuel designs.

1.0 INTRODUCTION, SCOPE, AND OBJECTIVE

GE¹ fuel product lines have continually evolved over the last 20 years, including innovations in spacer designs. Spacers provide a necessary mechanical function (e.g., support and separation of fuel pins), and play an important role in terms of critical power and pressure drop performance. Fuel critical power and ΔP performance characteristics are experimentally confirmed from full-scale thermal-hydraulic testing, using electrically heated replicas of the fuel bundles. The pressure drop testing is used to develop spacer loss coefficients, which are ultimately used in design calculations and monitoring applications.

In order to model and predict ΔP in a fuel bundle, the void fraction must be accurately predicted. The analytic expression used to evaluate the elevation pressure drop uses void fraction (directly) as a variable. Furthermore, in BWR applications, the correct modeling of fuel pressure drop, flow rate, and axial power shape all depend on the accuracy of the void prediction due to the strong void/power feedback mechanism present in the reactor. One of GNF's approved methods for predicting void fraction is the Findlay-Dix void correlation. The Findlay-Dix correlation is based on the drift-flux model. It is applied in one-dimension, providing a planar average void fraction as a function of steam properties (a function of temperature and pressure), void fraction, and a Reynolds number (dimensionless) based on the bundle flow rate. The Reynolds number, which represents the ratio of inertial to viscous forces, is calculated based on a characteristic length scale, i.e., the hydraulic diameter (D_H).

The objective of this analysis is to assess the bias and uncertainty in the steady state void fraction values predicted by the Findlay-Dix correlation. The evaluation is based on comparisons of calculated ΔP to the experimental ΔP measurements obtained for the GE14 and GNF2 fuel bundle designs. These bundle designs represent current (in-service) fuel and a new design, both of which are based on 10x10 lattices. The designs are comparable (axially dependent $D_H \approx 0.39$ to 0.55 inches), but different with respect to the locations and heights of the partial length fuel rods. The basis of this analysis is that error in the void prediction can be estimated by establishing a relationship between void fraction error and ΔP error (calculated minus measured ΔP)². The estimated error can then be compared with results from the original Findlay-Dix validation database in order to judge the adequacy of the correlation for 10x10 designs.

In general, it has been demonstrated that drift-flux type correlations predict both steady state and transient data well, including rapid transients [10]. However, transient void fraction prediction accuracy is not within the scope of this analysis. Transient void predictions are important for determining the correct dynamic response of reactor cores, as well as limiting channel performance. While transient two-phase flow predictions may utilize the void correlation, the adequacy of the results is also highly dependent on the formulation of the

¹ General Electric or simply "GE" is used in this document to refer to the Company and its affiliates, specifically Global Nuclear Fuel, Americas (GNF-A).

² While the main purpose of the fuel product ΔP tests was to determine spacer loss coefficients, this exercise is very similar to one of the popular techniques that have been applied to establish basic void fraction data. Historically, void fraction data has been experimentally determined based on measured elevation pressure drop data (subtracting a frictional component).

NEDO-33173, Supplement 1
Non-proprietary Version

conservation equations, their numerical treatment, and other supporting models (e.g., heat transfer). Recognizing that these predictions are the product of a particular “equation and correlation set,” GNF’s methodologies for transient and accident evaluations have their own qualification bases³ supporting regulatory approval. These bases support implementation of all the relevant models, including the drift flux model (void correlation) as appropriate.

³ Methodologies are typically implemented as computer “codes,” which are qualified for specific applications, such as Peak Clad Temperature (PCT) predictions in Loss-of-Coolant Accident (LOCA) evaluations and Minimum Critical Power Ratio (MCPR) predictions in Anticipated Operational Occurrence (AOO) evaluations. The relevant physical phenomena and response variables of interest (e.g., PCT or MCPR) drive the required accuracy and unique sensitivities to the various component models, which are considered in the code validation process.

2.0 ASSUMPTIONS

The following assumptions are applicable to this analysis:

- Measurement bias is assumed to be zero. Any systematic error (net error) between predicted and measured pressure drops is assigned to an error in the void fraction calculation/prediction (for the purpose of this analysis). This is discussed further in Sections 4.2 and 5.0.
- Measurement errors are assumed to be random (and normally distributed). Similarly, the void fraction uncertainties are assumed to be normal.
- Two-phase losses due to sudden expansions or contractions have been ignored as small relative to other losses.
- Fluid properties are evaluated at system pressure (i.e., the change in saturated liquid and vapor densities due to the pressure drop within the bundle is ignored). In addition, the system pressure measurement in the experiments [[

]]

This slight variation is ignored in the void error estimate. However, the ISCOR evaluations [1] used the measured system pressure (and subcooling) values reported for each test run.

- The expression used in this analysis for the elevation pressure drop considers the fluid properties at saturation conditions (i.e., $\rho_f \approx \rho_{liq}$) throughout the bundle.
- Reference [1] give calculated versus measured pressure differences for a series of experimental runs. Errors associated with the calculational model (e.g., differences between the as-modeled geometry and the experiment) are assumed to be small and are ignored.
- The calculational uncertainty and measurement errors are treated as independent (i.e., uncorrelated). This is discussed further in Section 4.4.

There are no other assumptions for this analysis.

3.0 APPROACH AND METHODS

The approach used in the analysis is to relate the differences between experimentally determined ΔP measurements and ΔP calculations to potential errors in predicted void fraction. The necessary relations are developed in Section 4.0. The results of the comparison can be used to draw general conclusions regarding the magnitude of errors associated with the application of the Findlay-Dix void correlation to 10x10 fuel designs (e.g., GE14 and GNF2). No Engineering Computer Programs (ECPs) were used in this evaluation. However, as noted in Section 2.0, the comparisons used as input to this analysis were based on ISCOR calculations. Microsoft Excel 2000 (version 9.0.4402 SR-1), standard spreadsheet software, was used to perform some simple calculations and create the figures in Section 4.0 and 5.0 from tabular data. Minitab Release 12.2 was used to compile summary statistics based on the GE14 and GNF2 pressure drop datasets.

4.0 ANALYSIS AND RESULTS

4.1 Predicted Versus Measured ΔP

Pressure drop predictions compared to full-scale test data are presented in references [1] and [2]. In these reports, families of curves (predicted versus measured ΔP) for various power levels and mass flow rates at [[]] are shown. The results can be summarized as shown in Figure 4-1 and Figure 4-2. The test conditions and statistics corresponding to the figures are summarized in Table 4-1.

[[

]]

Figure 4-1. GE14 Pressure Drop Comparisons

[[

]]

Figure 4-2. GNF2 Pressure Drop Comparisons

Table 4-1. Predicted Versus Measured Data Summary – Spacer ΔP Tests [1]

Test Set		Test Ranges				Results	
Bundle Design	No. Points	Power (MWt)	Mass Flux (Mlbm/hr-ft ²)	System Pressure (psia)	Inlet Temp (°F)	Ave. ΔP_{cal} - ΔP_{meas} (psid)	Std. Dev. (psid)
[[
]]

Pressure drop tests are conducted in conjunction with critical power testing for fuel product lines. Consequently, the choice of radial peaking pattern and Axial Power Shape (APS) is primarily driven by needs associated with the critical power data. However, this is of little

consequence, since the data is based on full-scale tests and completely applicable for assessing pressure drop performance. The test bundles are electrically heated replicas of the actual fuel designs. It is worth noting that the main purpose of the ΔP test series was to develop spacer loss coefficients, i.e., they were not designed specifically for examining the accuracy of the void correlation. This point will be discussed further in Section 5.0.

The ΔP data is from two “test assemblies.” The two assemblies were configured into a variety of peaking patterns for the experiments. [[

]]

Both Figure 4-1 and Figure 4-2 show the 0 MWt data separate from the 1 MWt and greater data. This highlights the fact that while these points are part of the original datasets, they are un-voided and removed from the void error analysis (see Section 4.5). Examining the separate data is also interesting in that it highlights the agreement based on the choice of single-phase loss coefficients and two-phase multipliers. The agreement is excellent at 0 MWt with the single-phase loss coefficients (alone), as well as at the higher power levels with the two-phase multipliers applied.

4.2 Pressure Drop Bias and Uncertainty

A pressure drop calculation can be considered to include an error or bias (δP). Correlations could (potentially) be a source of error, as well as approximations or assumptions inherent in the method and numerical errors (truncation and round-off). The bias may not be constant; it may change for different conditions and it may be positive or negative. For a particular set of boundary conditions, geometry, etc., (i.e., *for a particular instance or calculation*) the pressure drop can be written

$$\Delta P_{Tot.Calc} = \sum_i \sum_j (\Delta P_{i,j} + \delta P_{i,j}) = \Delta P_{Tot} + \sum_i \delta P_{Calc,i} \quad (4.1)$$

Equation (4.1) is shown in a form consistent with the ISCOR code, in the sense that pressure loss terms may be summed over each axial node “j” for each type of loss “i” (acceleration, friction, etc.).

Similar to Equation (4.1), a measured pressure drop or test run can also be shown with error terms. Any given measurement may contain a systematic bias, as well as a contribution due to random error ($\pm \epsilon$). However, in this analysis, the measurement bias is assumed to be zero.

$$\Delta P_{Tot.Meas} = \Delta P_{Tot} + \cancel{\delta P_{Meas}} \pm \epsilon_{Meas} \quad (4.2)$$

⁴ The GNF2 fuel bundle designed for domestic BWR/4-6 plants has [[

]]

NEDO-33173, Supplement 1
Non-proprietary Version

Measurement bias is minimized (eliminated) by good experimental practices (e.g., calibration of pressure gages, etc.). Subtracting Equations (4.1) and (4.2) gives

$$\Delta P_{Tot,Calc} - \Delta P_{Tot,Meas} = \sum_i \delta P_i \pm \varepsilon_{Meas} \quad (4.3)$$

where the subscript “*Calc*” has been dropped from the bias term.

4.3 Calculated Steady State Void Fraction Bias

The calculated steady state pressure drop can be expressed in terms of its components. Expanding Equation (4.1) for steady-state conditions and considering totals for the channel (of each loss type “*i*”)

$$\Delta P_{Tot,Calc} = \Delta P_{Elev} + \Delta P_{Exp/Con} + \Delta P_{Fric} + \Delta P_{Loc} + \Delta P_{Acc} + \sum_i \delta P_i \quad (4.4)$$

The total steady state pressure drop consists of components due to elevation, friction, local losses, acceleration, and sudden expansions or contractions (another form of acceleration loss). [[

]] Also, in the pressure drop experiments of interest, there is no power feedback from void fraction changes. Therefore, the calculated void fraction does not influence the axial power and predicted quality profile through the bundle.

[[

]] (4.5)

For the purposes of this analysis, all of the calculational bias will be assumed to be due to errors in the void fraction.

$$\delta P_{Fric} = \delta P_{Loc} = \delta P_{Acc} = 0 \quad (4.6)$$

For convenience, the analytic expressions for the terms in Equation (4.4), i.e., the formulas for the pressure drop components, are presented in APPENDIX B.

For the purpose of this calculation, the expansion / contraction term is relatively small and may be neglected. There may be a substantial expansion at the exit of an actual BWR bundle (where the rodded region ends). However, this is not true of the test section, which is shown in Figure 2 of reference [1]. The upper pressure tap is still within a rodded region, where the area change is less dramatic than the bundle exit.

$$\delta P_{Exp/Con} \approx 0 \quad (4.7)$$

NEDO-33173, Supplement 1
Non-proprietary Version

Under these assumptions, the error term (δP) in Equations (4.3) and (4.4) reduces to a single term related to elevation head.

$$\delta P = \Delta P_{Tot,Calc} - \Delta P_{Tot,Meas} \pm \varepsilon_{Meas} \quad (4.8)$$

Again, any systematic error has been assumed to be due to the calculated void fraction.

The two-phase elevation pressure drop is given by

$$\Delta P_{Elev,Calc} = \frac{\bar{\rho} g \Delta z}{g_c} = \frac{g \Delta z}{g_c} [\bar{\alpha} \rho_g + (1 - \bar{\alpha}) \rho_{liq}] \cong \frac{g \Delta z}{g_c} [\bar{\alpha} \rho_g + (1 - \bar{\alpha}) \rho_f] \quad (4.9)$$

Equation (4.9) is written in terms of the total two-phase elevation pressure drop, so the void fraction (α) is shown with a bar to indicate that this is an average over the volume being modeled. In this sense, the void fraction value represents the relative volumes of fluid and vapor over the length (Δz) between (simulated) pressure taps.

If the error in the calculated elevation head is assumed to be due to the void fraction calculation, then Equation (4.9) can be expanded to include error terms. Introducing a small perturbation by substituting $\bar{\alpha} + \delta \bar{\alpha}$ for void fraction and $\Delta P + \delta P$ for pressure drop in Equation (4.9) gives

$$\Delta P_{Elev,Calc} + \delta P = \frac{g \Delta z}{g_c} \{ (\bar{\alpha} + \delta \bar{\alpha}) \rho_g + [1 - (\bar{\alpha} + \delta \bar{\alpha})] \rho_f \} \quad (4.10)$$

Rearranging terms gives

$$\Delta P_{Elev,Calc} + \delta P = \frac{g \Delta z}{g_c} [\bar{\alpha} \rho_g + (1 - \bar{\alpha}) \rho_f] + \frac{g \Delta z}{g_c} (\rho_g - \rho_f) \delta \bar{\alpha} \quad (4.11)$$

Comparing Equation (4.11) to (4.9), or subtracting, gives an expression relating the void error to a pressure drop error

$$\delta \bar{\alpha} = \frac{g_c \delta P}{g \Delta z (\rho_g - \rho_f)} \quad (4.12)$$

Substituting Equation (4.8) for δP gives an expression in terms of the calculated minus measured pressure drop

$$\delta \bar{\alpha} = \frac{g_c (\Delta P_{Tot,Calc} - \Delta P_{Tot,Meas} \pm \varepsilon_{Meas})}{g \Delta z (\rho_g - \rho_f)} \quad (4.13)$$

Under these assumptions, the error in the predicted (average) void fraction in a bundle is only dependent on the difference between the calculated and measured pressure drop, the elevation difference between pressure taps (assumed to be well modeled in the calculation), the saturated liquid and vapor densities, and a contribution from a random measurement error. Taking an

average over a collection of “N” observation-prediction pairs gives an expression for the mean error (bias) in void fraction

$$\overline{\delta\bar{\alpha}} = \frac{1}{N} \sum_i^N \delta\bar{\alpha}_i = \frac{g_c}{g\Delta z(\rho_g - \rho_f)} \frac{1}{N} \sum_i^N (\Delta P_{Tot,Calc,i} - \Delta P_{Tot,Meas,i} \pm \varepsilon_i) \quad (4.14)$$

If the measurement error is normally distributed, as the sample size increases, the sum of the errors decreases and the average becomes a better estimate of the mean.

$$\overline{\delta\bar{\alpha}} = \frac{1}{N} \sum_i^N \delta\bar{\alpha}_i = \frac{g_c (\overline{\Delta P_{Tot,Calc} - \Delta P_{Tot,Meas}})}{g\Delta z(\rho_g - \rho_f)} \quad (4.15)$$

In the right-hand side of Equation (4.15), the random error term has been dropped, i.e., $\frac{1}{N} \sum \pm \varepsilon_i \rightarrow 0$ as N becomes large (i.e., positive and negative errors are equally likely).

4.4 Void Fraction Uncertainty Treatment

4.4.1 Approach

The void bias described by Equation (4.15) is a function of two variables, calculated and measured pressure drop. The right hand side of the equation represents the average pressure drop error or bias. The uncertainty in this value can be written as a sum of errors from the two independent sources

$$\sigma_{\Delta P}^2 = \sigma_{Calc}^2 + \sigma_{Meas}^2 \quad (4.16)$$

The left hand side of Equation (4.16) can be obtained from the calculated minus measured pressure drops, i.e., a calculation of the standard deviation based on the calculation-measurement pairs. Letting $x = \Delta P_{Tot,Calc} - \Delta P_{Tot,Meas}$, the uncertainty in “x” can be estimated as the standard deviation of a sample [7]

$$\sigma_{\Delta P}^2 \approx s^2 = \frac{1}{N-1} \sum_i^N (x_i - \bar{x})^2 \quad (4.17)$$

The measurement uncertainty may be obtained from information in reference [1]. Once two of the three quantities are established, the remaining uncertainty can be determined.

The terms in (4.16) can be combined using the propagation of errors [7] technique.

$$\sigma_x^2 = \left(\frac{\partial x}{\partial u}\right)^2 \sigma_u^2 + \left(\frac{\partial x}{\partial v}\right)^2 \sigma_v^2 + \dots + \left(\frac{\partial x}{\partial z}\right)^2 \sigma_z^2 \quad (4.18)$$

In order to apply this technique, expressions for sensitivity coefficients (derivatives) are necessary. These coefficients can be derived from the relationships presented in Section 4.3.

Equations (4.16) and (4.18) represent the case of independent (uncorrelated) errors. The predicted versus measured results presented in Section 4.1 are well correlated. However, the

existence of correlation between two variables does not imply causality. For the most part, the experimental ΔP values are not used as inputs to the pressure drop calculations. [[

]] In other words, the single-phase spacer loss coefficients were derived to best match a subset of the measured data, so there is a possibility of correlated errors between these points that is ignored. In contrast, the GNF2 spacer loss coefficients were projected from an area scaling analysis applied to the GE14 spacer geometry. The GNF2 loss coefficients were determined a priori and the ΔP testing was confirmatory. The analysis demonstrates that the selected loss coefficients are optimal. Furthermore, the Findlay-Dix void prediction (i.e., the assumed source of calculational error) is based on a completely different experimental database, independent of the 10x10 ΔP measurements. For these reasons, the errors are treated as uncorrelated.

4.4.2 Void and ΔP Relationship

Using the assumptions employed to derive Equation (4.13), it is only necessary to evaluate a term for the elevation pressure loss in order to evaluate the calculational uncertainty

$$\sigma_{\Delta P}^2 = \left(\frac{\partial(\Delta P)}{\partial \bar{\alpha}} \right)^2 \sigma_{\bar{\alpha}}^2 + \sigma_{Meas}^2 \quad (4.19)$$

The sensitivity coefficient can be obtained by differentiating Equation (4.9). Substituting and rearranging gives

$$\sigma_{\bar{\alpha}} = \pm \frac{\sqrt{\sigma_{\Delta P}^2 - \sigma_{Meas}^2}}{\left(\frac{\partial(\Delta P)}{\partial \bar{\alpha}} \right)} = \pm \frac{\sqrt{\sigma_{\Delta P}^2 - \sigma_{Meas}^2}}{\left[\frac{g\Delta z}{g_c} (\rho_g - \rho_f) \right]^2} = \pm \frac{g_c \sqrt{\sigma_{\Delta P}^2 - \sigma_{Meas}^2}}{g\Delta z (\rho_g - \rho_f)} \quad (4.20)$$

This approach for treating uncertainty produces a similar result (in terms of form) to Equation (4.12), since consistent assumptions have been applied. However, in order to solve (4.20), an expression or estimate for the measurement uncertainty is necessary.

4.4.3 Measurement Uncertainties in the ΔP Experiments

The pressure drop uncertainties for the GE14 experimental series are given in terms of the measured test parameters (e.g., flow rate, system pressure, etc.). These values can be used to estimate the total measured ΔP uncertainty. [[

]]

[[

]] This uncertainty value is much smaller than the GE14 value and may be neglected.

4.5 Void Error Estimate

4.5.1 Void Fraction Bias and Uncertainty Based on GE14 Data

Appendix A of reference [1] provides a tabular summary of pressure drop comparisons for GE14 fuel. The last column of the table contains calculated minus measured pressure drops for each (steady-state) experimental run. The table also contains a mean bias and standard deviation value for the entire data set [[]]. Removing the 0 MWt data, the summary statistics are shown in Figure 4-3.

[[

]]

Figure 4-3. GE14 Pressure Drop Statistics

The mean bias [[]] can be related to void fraction using (4.15). Neglecting slight changes in the system pressure in the test runs and evaluating [[]]

⁵ The input data from reference [2] is based on [[]] of the test section.

]] of

[[

(4.21)

]]

Using Equation (4.20) gives an estimate of the [[

(4.22)

GE14]]	(4.23)
------	----	--------

This information may be compared to the original Findlay-Dix void correlation statistics.

4.5.2 Void Fraction Bias and Uncertainty Based on GNF2 Data

The exercise can be repeated for the GNF2 dataset using tabular data. Removing the 0 MWt data, the summary statistics are given in Figure 4-4.

[[

]]

Figure 4-4. GNF2 Pressure Drop Statistics

Using Equation (4.15) again

[[

(4.24)

]] of the test section. Using Equation (4.20) to estimate the uncertainty

[[(4.25)

GNF2]] (4.26)
------	-----------

This information may be compared to the original Findlay-Dix void correlation statistics.

4.6 Comparison to the Findlay-Dix Correlation Database

The Findlay-Dix correlation was developed based on sets of simple geometry and multi-rod data. Once the correlation was established, it was [[It provides a convenient basis for comparison with the 10x10 based data.

Table 4-2. Multi-Rod Experimental Data Used to Validate The Findlay-Dix Correlation

Data Series	No. of Points	Average Error ⁶	Std. Deviation
[[
]]

⁶ The average error is defined as $\Delta\alpha = \alpha_{Meas} - \alpha_{Calc}$

⁷ Combined using a weighted average for the mean $\bar{x} = (n_1\bar{x}_1 + n_2\bar{x}_2)/(n_1 + n_2)$ and a pooled standard deviation $\sigma_p^2 = [(n_1 - 1)\sigma_1^2 + (n_2 - 1)\sigma_2^2]/(n_1 + n_2 - 2)$, where the data series are treated as sharing a common variance.

⁸ The 95% confidence interval for the mean is given by $\bar{x} \pm \frac{z_{\alpha/2}}{\sqrt{n}} \sigma_p = \bar{x} \pm \frac{1.96}{\sqrt{n}} \sigma_p$ (large sample). The 95% confidence interval for σ is given by the range

$$\left[\frac{(n-1)\sigma_p^2}{\chi_{\alpha/2, n-1}^2} \right]^{1/2} \text{ and } \left[\frac{(n-1)\sigma_p^2}{\chi_{1-\alpha/2, n-1}^2} \right]^{1/2} = [[]]$$

NEDO-33173, Supplement 1
Non-proprietary Version

Note that the average error in Table 4-2 is defined as measured versus calculated, which is opposite the ΔP data. Correcting the sign convention, the mean error values presented in Equations (4.23) and (4.26) are consistent. [[

(4.27)

]]

⁹ Typically, in hypothesis testing, the null hypothesis is “equal values” and the alternate hypothesis is “non-equal values.” The “P value” is typically taken as the smallest level of significance that would lead to rejection of the null hypothesis, which is usually compared to a α value (e.g., 0.05 for 95% confidence).

5.0 EVALUATION, SUMMARY, AND CONCLUSIONS

5.1 General

The Findlay-Dix void correlation has been examined based on pressure drop data for two 10x10 fuel designs. The conditions examined are [[
]]. The experiments included [[

]]. The void fraction bias and uncertainty determined from these tests appear to be consistent with the original Findlay-Dix correlation database. A statistical comparison does not suggest that the bias and uncertainty determined from the pressure drop data are different from the correlation database. This would be expected based on the consideration that the range of hydraulic conditions (pressure, void fractions, and Reynolds numbers) and [[

]]

The 10x10 designs examined in this study utilize Partial Length Rods (PLRs) as a design feature. The results presented here indicate that void fraction is well predicted, consistent with the more detailed evaluation presented in reference [13], [[

]]

5.2 Impact of Key Assumptions on Conclusions

Equation (4.6) in Section 4.3 introduced a key assumption into the evaluation. In this analysis, the net calculational error has been assigned to the void fraction prediction through the elevation head term. However, in reality, the other calculational errors may not be zero.

$$\delta P_{Fric} \neq 0, \quad \delta P_{Loc} \neq 0, \quad \delta P_{Acc} \neq 0 \quad (5.1)$$

This raises a concern for compensating errors in the calculation. Unfortunately, the individual ΔP components cannot be resolved through direct comparisons to the GE14 and GNF2 test data. These experiments are integral tests. All of the pressure loss physical mechanisms are together (confounded) in the measurements, so it is not possible to directly compare calculations to the constituent terms.

In order to address this issue, it would be desirable to determine how much of the calculated error is due to the void fraction prediction, as opposed to the frictional/acceleration loss components. Alternatively, examining the predictions versus data provides evidence that

$$|\delta P_{Fric} + \delta P_{Loc} + \delta P_{Acc}| \gg |\delta P_{Elev}| \quad (5.2)$$

(i.e., that the calculated frictional and/or acceleration loss terms dominate the calculated error for the overall dataset). With this information, it would still not be possible support claims regarding the exact magnitude of the void error. However, this would support a conclusion that

NEDO-33173, Supplement 1
Non-proprietary Version

the void uncertainty has been conservatively estimated by the process detailed in Section 4.0, which supports the results of the comparison to the original validation datasets. Since the source of error can be distinguished as shown in Equation (5.2), an exact breakdown of the constituent pressure drops is not necessary (for a relative comparison of void error). It is possible to gain more insight into the source of the errors by considering additional information:

1. Trend analysis and parameter sensitivities – Elevation pressure drop decreases linearly with increasing void fraction, as shown by Equation (4.9). A column of solid water weighs more than a column of vapor, and the intermediate states are a simple function of the volume fraction. Also, the total pressure drop increases with increasing void fraction (or bundle power-to-flow ratio) due to other mechanisms. These known trends can be used to evaluate the errors, and ultimately to evaluate the validity of Equation (5.2).

Note that the conversion between calculated void and ΔP errors is only a function of density and elevation (i.e., does not vary with void fraction), as shown by Equation (4.12). So the conversion does not “amplify” calculated void errors. A $\delta P = 0.19$ psid measured error equates to a $\Delta\alpha = 0.05$ calculated error at either 10% or 90% void fraction. This is illustrated in Figure 5-1.

2. Correlation analysis – The residual errors (ΔP errors) can be fit to parameters such as mass flux and power-to-flow ratio (proportional to exit or average void fraction). The degree of correlation (goodness of fit characterized by r^2) can be taken as evidence of a relationship, or a lack of a relationship. Correlation analysis does not imply causality or reveal underlying reasons for causal relationships, but can be used to determine when relationships exist.
3. Experimental bases – The bases for the expressions used to determine the pressure loss components provide the assurance that these calculational errors are minimized and not prone to compensating errors. The current design method ΔP correlation set originated from a test program based on [[

]] facilities. These tests (including single-phase, two-phase, adiabatic and diabatic measurements, as well as ΔP measurements between spacers) were used to resolve the individual pressure drop components (acceleration, friction, elevation, and local losses) and established the basis for Method B. The tests were also used to prove that the pressure drop correlations scale well with D_H .

Items 1 and 2 (above) relate to the data under consideration in this analysis and are discussed below.

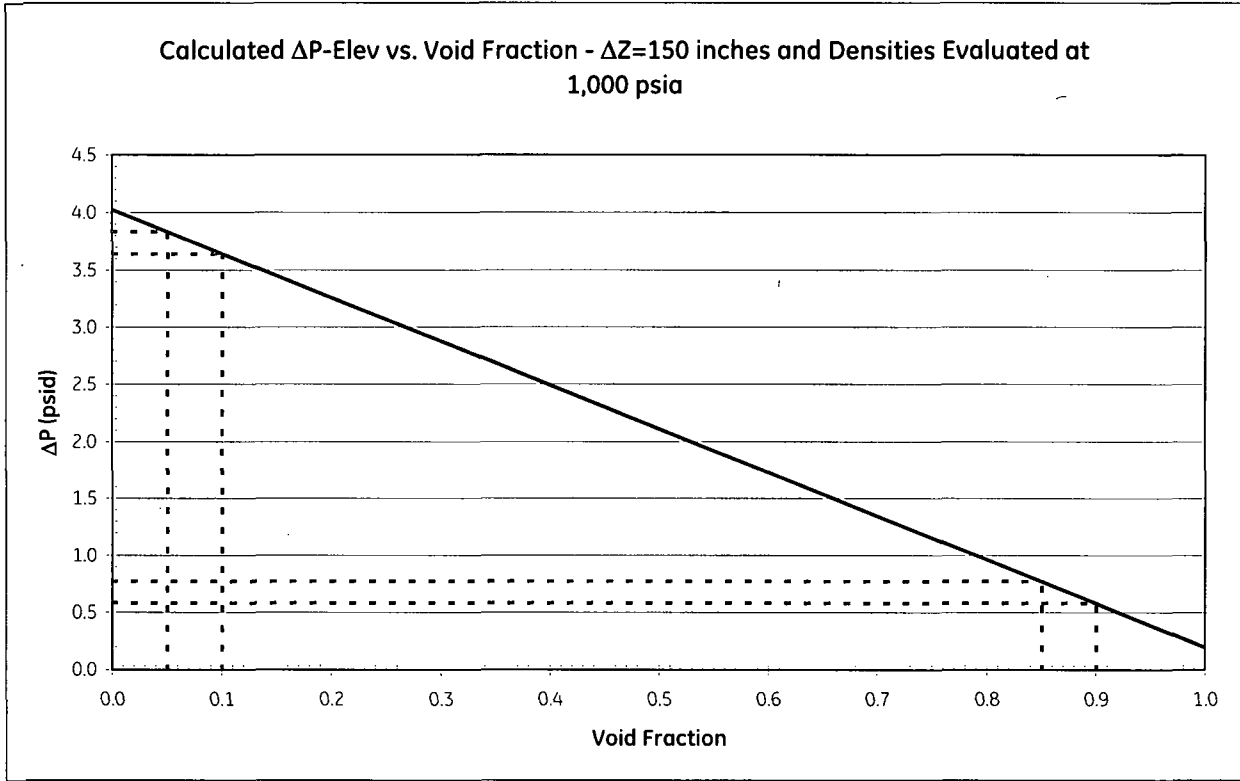


Figure 5-1. Calculated Elevation ΔP Versus Void Fraction Based on Equation (4.9)

5.2.1 Trend Analysis

Figure 5-2 shows predicted and calculated pressure drops for the GE14 tests. Figure 5-3 shows a comparable graph for GNF2 (identical trends). [[

]]

[[

]]

Figure 5-2. GE14 ΔP Data Predicted with Method B [1]

[[

]]

Figure 5-3. GNF2 ΔP Data Predicted with Method B

If the ΔP error is primarily driven by a void fraction discrepancy or miscalculation, then the errors could be expected to correlate to power-to-flow ratio. Furthermore, given the fact that the total ΔP generally increases with power-to-flow ratio, the postulated void error would need to increase with void fraction in order to explain the observed behavior.

If the calculated error is primarily a function of the mass flux (e.g., friction, local losses, or acceleration), then a squared relationship could be expected. Frictional losses are typically (empirically) correlated to the square of mass flux (velocity or mass flow rate).

5.2.2 Correlation Analysis

[[

]]

[[

]]

Figure 5-4. Pressure Drop Error (δP) Versus Power-to-Flow Ratio

[[

]]

Figure 5-5. Pressure Drop Error (δP) Versus Mass Flux

[[

(5.3)

]]

5.3 Integral Versus Local Errors

The ΔP error values that serve as the basis for this analysis are essentially based on the cumulative ΔP (and in a sense, cumulative error) over the test section. This was done primarily to maintain consistency with the base analyses [1] and [2]. However, as a consequence, this raises another concern for the potential impact of compensating errors and requires examination. A review of the data does not indicate that this is a concern. Figure 5-6 shows the axial detail for a representative GNF2 test comparison. The figure shows the calculated cumulative ΔP compared to the summed test data from individual pressure taps, as well as the calculated void fraction (based on Findlay-Dix), which is plotted on the opposite axis (for reference). It is interesting to note that in this case, [[

]]
[[

]]

Figure 5-6. GNF2 ΔP (Calculated or Measured) Versus Elevation

Figure 5-6 shows that the calculation generally agrees well with the pressure tap data at the various elevations. In that regard, this is a representative case. The worst agreement for this particular case is [[

]]

An interesting feature of the GNF2 bundle is that [[

]]

Figure 5-7 is similar to Figure 5-6 (the format and scales for the axes are the same), but shows three GNF2 test runs instead of one. These curves correspond to the very low flow rate (low Re) cases, where elevation head tends to dominate the total pressure drop. In these cases, elevation head is more than 80% of the total calculated pressure drop through the channel. For test run 627, elevation head is 89% of the total calculated in-channel ΔP . Although the relative magnitudes of the constituent δP errors are unknown for this subset of data, the frictional contribution should be low.

[[

]]

Figure 5-7. GNF2 ΔP (Calculated or Measured) Versus Elevation for Low Flow Rate Test Runs

5.4 Confirmatory Low Flow Data Subsets

Figure 5-8 shows some of the same data as Figure 5-2, only more focused on the low flow “tails” of the curve set. The figure shows that the total pressure drop for the < 3 MWt, < 0.3 lbm/hr-ft² data actually dips below the 0 MWt pressure drop data. In these cases, friction is relatively low and introducing voids reduces the average water density, which reduces ΔP_{elev} and causes a net reduction in the total pressure drop relative to the single-phase (0 MWt) case. This subset of 6 points has the lowest frictional pressure loss (i.e., the components due to friction, local, and acceleration losses, or $\Delta P \propto G^2$) of the GE14 test set. For these cases, properly calculating the contribution from elevation head is very important for accurately predicting the total ΔP .

[[

]]

Figure 5-8. GE14 ΔP (Calculated or Measured) Versus Mass Flux for the 0 to 3 MWt Test Runs

Table 5-1 provides a data summary for the low flow subsets. The GNF2 test runs from Figure 5-7 are included in the table, as well as the comparable GE14 data points. The δP column in the table gives the calculated minus measured pressure drop for each test run, consistent with Equation (4.3). The $\delta \bar{\alpha}$ column gives the calculated void error, consistent with Equations (4.21) and (4.24).

Table 5-1. Low Flow Rate ΔP Test Summary [1]

Bundle Type / Run	Power (MWt)	Mass Flux (Mlbm/hr-ft²)	Pressure (psia)	T_{inlet} (°F)	δP (psid)	Calculated $\delta\bar{\alpha}$
[[
]]

The “low flow” datasets were selected based on the power and flow combinations that maximized the elevation head contribution to the total ΔP . At 1 MWt with the various flow rates in, the calculated ΔP_{elev} is 80% or more of the total pressure drop. The elevation pressure drop in the 3 MWt cases is roughly 50% of the total pressure drop through the channel. In all of these cases, the frictional pressure drops are relatively small. Given the excellent agreement for the single-phase predictions shown in Figure 5-8, pressure drop errors are more likely to be associated with the calculated void fraction and elevation head than the calculations for the other losses. Higher power levels and flow rates are much more typical of BWR operating conditions. However, these conditions tend to increase the frictional, local, and acceleration pressure drop contributions so that they dominate over elevation head.

Table 5-2 gives a summary of the average errors, standard deviations, and confidence intervals for the calculated void error values from Table 5-1. The standard deviation in $\delta\bar{\alpha}$ is a straightforward calculation with no adjustment for measurement uncertainty, i.e., the value is not based on Equation (4.20).

Table 5-2. Low Flow Rate Calculated Void Bias and Standard Deviation

Statistic or Confidence Interval (C.I.)	GNF2	GE14
[[
]]

Examining Table 5-2, the GNF2 and GE14 mean bias and uncertainty values are not significantly different from each other. Even without performing hypothesis tests, it is evident that there is significant overlap in the confidence intervals. The parent samples for the two bundle designs are different (one sample is non-normal). However, based on the results of the trend and correlation analysis, this appears to be due to the fact that the GE14 sample has more high power, high flow rate comparison points, which show some distinct δP bias. Both the GE14 and GNF2 low flow $\delta\bar{\alpha}$ subsets are normally distributed¹².

It is interesting to compare the GE14 and GNF2 low flow data subsets with the Findlay-Dix validation data shown in Table 4-2. The mean errors and standard deviations can be compared using hypothesis tests. The sample sizes are small (6 points), but this impact is appropriately captured in the degrees of freedom that determine the acceptance intervals for the test statistics. The tests indicate that both the GE14 and GNF2 low flow uncertainties (variances) are different from the validation data (slightly smaller) at the 95% confidence level. A summary of comparisons is shown in Table 5-3.

¹⁰ Confidence interval based on a random sample from a normal population with an unknown variance.

¹¹ Confidence interval based on a random sample from a normal population.

¹² Based on an Anderson-Darling or Kolmogorov-Smirnov (χ^2 based) tests with $\alpha = 0.05$.

Table 5-3. Low Flow Rate Data Test Comparisons

Hypothesis	Test Statistic	Acceptance Interval and Result
[]		

Hypothesis	Test Statistic	Acceptance Interval and Result
]]

The low flow data represents a subset of available 10x10 ΔP data. The void bias and uncertainty derived from the low flow data can be compared with the ASEA tests, consistent with the treatment applied to the larger (parent) datasets. The conclusions based on this data are confirmatory and consistent with the rest of the analysis. The GE14 and GNF2 (low flow) subsets are different from the original validation data. The low flow uncertainties appear to be slightly smaller. The parent (full) datasets have larger uncertainties. However, the parent datasets include additional contributions to the variance from the frictional terms. Nonetheless, even with the additional error contributions, the GNF2 uncertainty based on the entire dataset is not significantly different from the validation data (Section 4.6).

5.5 Summary

The key points from this analysis can be summarized as follows.

- The GE14 and GNF2 pressure drop tests are representative of current 10x10 fuel designs. In addition, the tests cover a very wide range of power-to-flow ratios, some of which approached the critical power for the ΔP test conditions. [[
]] The test points were selected for broad application to the operating BWR fleet.
- Relating pressure drop error to a calculated void fraction error, comparisons to 10x10 bundle ΔP data do not indicate that void bias and uncertainty are greater than the original Findlay-Dix correlation database.

NEDO-33173, Supplement 1
Non-proprietary Version

- Correlation analysis indicates that the calculated pressure drop errors for the overall datasets are dominated by the frictional and/or acceleration terms, not the elevation (void) term as assumed for the purpose of the analysis.

The fact that the frictional/acceleration errors appear to dominate the total calculated error, but have been included in the ΔP assigned to the elevation pressure drop, adds some confidence that the void fraction bias and uncertainty are actually smaller than the values determined in this analysis. The 10x10 void errors have been over predicted, yet the uncertainties are not distinctly different from the values based on the original validation datasets. The low flow data subsets, where the frictional contribution to error is minimized, provide additional confirmation. The low flow subset uncertainties are smaller than the validation data uncertainties. All of these observations support an important conclusion regarding the 10x10 pressure drop data. The data does not suggest that the void correlation bias or uncertainty have increased between 8x8 and contemporary fuel designs.

For BWR applications, the composition of the correlation database (e.g., tubes versus rod arrays, or array size 8x8, 9x9, or 10x10) does not appear to impose a performance limit or constraint. This is consistent with findings from other investigators. Coddington and Macian [10], in their assessment of void correlation performance, report that two correlations based solely on tube data produced standard deviations as low as the best rod bundle based correlations. It is also interesting to note that in this study, the Dix correlation (a predecessor to the Findlay-Dix correlation) was ranked in the "top five," based on bias and uncertainty derived from the datasets examined.

APPENDIX A. 1-D Flow Quality, Equilibrium Quality, and Void Fraction

A.1. Quality

Consider a simple (one-dimensional) heated channel or duct under steady state conditions. In this case, the energy storage rate is zero. The energy in-flow is equal to the energy out-flow.

$$\underbrace{\dot{m}e + \frac{d(\dot{m}e)}{dz} \delta z}_{OUT} = \underbrace{\dot{m}e + \dot{q}'(z) \delta z}_{IN} \quad (1.1)$$

Neglecting viscous dissipation, as well as the kinetic and potential energy changes, the energy per unit mass is simply the enthalpy. Integrating Equation (1.1) from the inlet to some arbitrary point ξ

$$[\dot{m}h]_{z=\xi} - [\dot{m}h]_{z=0} = \int_0^{\xi} \dot{q}'(z) dz \quad (1.2)$$

Considering the case where vapor is generated, conservation of mass can be written

$$\dot{m}_{out} = \dot{m}_{in} = \dot{m}_{Tot} = \dot{m}_g + \dot{m}_{liq} \quad (1.3)$$

The liquid may be subcooled in a general case, but the vapor phase is treated as saturated. Both phases are considered at the same pressure. Substituting, Equation (1.2) can be written

$$\dot{m}_g h_g + \dot{m}_{liq} h_{liq} = \dot{m}_{in} h_{in} + \int_0^{\xi} \dot{q}'(z) dz \quad (1.4)$$

where the “in” subscript indicates the channel inlet values at $z = 0$. Introducing the definition of flow quality

$$X = \frac{\dot{m}_g}{\dot{m}_g + \dot{m}_{liq}} \quad (1.5)$$

Equation (1.4) can be written

$$X h_g + (1 - X) h_{liq} = h_{in} + \frac{1}{\dot{m}_{Tot}} \int_0^{\xi} \dot{q}'(z) dz \quad (1.6)$$

In Equation (1.6), the liquid enthalpy and quality are functions of “z.” For subcooled boiling, another relation is necessary to partition the heat addition. Some energy is applied as sensible heat to raise the bulk fluid enthalpy, while the balance produces vapor. Regardless, the net energy addition to the fluid is strictly a function of the linear heat addition rate. Defining a bulk enthalpy for the two-phase mixture as

$$\bar{h}(z) = h_{in} + \frac{1}{\dot{m}_{Tot}} \int_0^{z=\xi} \dot{q}'(z) dz \quad (1.7)$$

Using (1.7), Equation (1.6) for the flow quality can be written in terms of enthalpy (energy addition)

$$X(z) = \frac{\bar{h}(z) - h_{liq}}{h_g - h_{liq}} \quad (1.8)$$

Under saturated conditions $h_{liq} = h_f$ and Equation (1.8) is equivalent to the thermodynamic equilibrium quality

$$X_c(z) = \frac{\bar{h}(z) - h_f}{h_g - h_f} = \frac{\bar{h}(z) - h_f}{h_{fg}} \quad (1.9)$$

Also, for saturated conditions, Equation (1.6) can be written

$$X = \frac{h_{in} - h_f}{h_{fg}} + \frac{1}{\dot{m}_{Tot} h_{fg}} \int_0^{z=\xi} \dot{q}'(z) dz \quad (1.10)$$

Equation (1.10) is a function of length (z). For the case where “z” equals the channel exit, the quality becomes the exit quality and the integral term is the total integrated channel power.

$$X_{exit} = \frac{\Delta h_{Sub}}{h_{fg}} + \frac{\dot{Q}}{\dot{m}_{Tot} h_{fg}} \quad (1.11)$$

In this derivation, no assumptions were necessary regarding the void fraction or relative velocities of the phases. Flow quality for the steady state case is determined solely on energy considerations (and conservation of total mass).

A.2. Void Fraction

A relationship between void fraction and flow quality can be obtained by introducing definitions for the mass flow rates of the phases (using bulk average quantities)

$$\dot{m}_g = \alpha \rho_g \bar{u}_g A \quad \text{and} \quad \dot{m}_f = (1 - \alpha) \rho_f \bar{u}_f A \quad (1.12)$$

Substituting these definitions into Equation (1.5) and rearranging gives

$$\alpha = \frac{1}{1 + \left(\frac{1 - X}{X} \right) \left(\frac{\rho_g}{\rho_f} \right) S} \quad (1.13)$$

where “S” is the slip ratio given by

NEDO-33173, Supplement 1
Non-proprietary Version

$$S = \frac{\bar{u}_g}{\bar{u}_f} = \left(\frac{1-\alpha}{\alpha} \right) \left(\frac{X}{1-X} \right) \left(\frac{\rho_f}{\rho_g} \right) \quad (1.14)$$

The slip ratio is the ratio of the average velocities of the phases. The drift flux model can be used to provide information about slip

$$\bar{u}_g = C_o j + \bar{v}_{gj} \quad (1.15)$$

where the superficial velocity (j) is given by

$$j = j_g + j_f = \alpha \bar{u}_g + (1-\alpha) \bar{u}_f \quad (1.16)$$

Using the relations in Equation (1.12) the superficial velocity can be written

$$j = \frac{\dot{m}}{A} \left[\frac{X}{\rho_g} + \frac{(1-X)}{\rho_f} \right] \quad (1.17)$$

Substituting $\alpha = X\dot{m}/\rho_g\bar{u}_gA$ (Equation (1.12) again) into Equation (1.14), then using (1.17), (1.15) and rearranging gives [9]

$$S = C_o + \frac{X\rho_f(C_o - 1)}{\rho_g(1-X)} + \frac{\rho_f\bar{v}_{gj}A}{\dot{m}(1-X)} \quad (1.18)$$

Recognizing that the last term can be neglected for many conditions of interest, Equation (1.18) allows quick, but reasonably accurate estimates of void fraction (only basic thermal-hydraulic parameters and information about C_o is required).

A.2.1. Example Based on GNF2 Data

Flow (or equilibrium) quality as described by Equation (1.11) varies with subcooling, power, and flow. The first term represents the sensible heat needed to achieve saturation conditions in the bulk liquid. The second term is directly proportional to power, and inversely proportional to mass flow rate. Referring to the GNF2 based data, it is reasonable to expect that a high (exit) quality value would be given by test run 651 (6 MWt and 75 klbm/hr), which has a relatively high power-to-flow ratio. Taking conditions at 1,000 psia and an inlet temperature of 525 °F, this equates to

$$X_{exit} = \frac{517.9 - 542.6 \frac{\text{Btu}}{\text{lbm}}}{650.4 \frac{\text{Btu}}{\text{lbm}}} + \frac{6 \text{ MWt}}{\left(75 \times 10^3 \frac{\text{lbm}}{\text{hr}} \right) \left(650.4 \frac{\text{Btu}}{\text{lbm}} \right) \left(2.93 \times 10^{-7} \frac{\text{MWt} - \text{hr}}{\text{Btu}} \right)} = 0.38 \quad (1.19)$$

For the approximation $S = 1$ (homogeneous flow), Equation (1.13) yields

NEDO-33173, Supplement 1
 Non-proprietary Version

$$\alpha_{exit} = \frac{1}{1 + \left(\frac{1-0.38}{0.38} \right) \left(\frac{2.24 \cancel{\text{lbm/ft}^3}}{46.32 \cancel{\text{lbm/ft}^3}} \right)} = 0.93 \quad (1.20)$$

which allows an estimate of C_o , where the distribution parameter is plotted for various pressures as a function of Re and void fraction. Estimating C_o graphically for high (e.g., 90%) void fraction gives [[

$$(1.21)$$

$$(1.22)$$

]]

A.2.2. Example Based on GE14 Data

Repeating the recipe in the previous example, the GE14 pressure drop experiments contained points at very high power-to-flow ratios. Considering the point at 5 MWt and 50 klbm/hr (run 473), the exit quality was

$$X_{exit} = \frac{517.9 - 542.6 \cancel{\text{BTU/lbm}}}{650.4 \cancel{\text{BTU/lbm}}} + \frac{5 \cancel{\text{MWt}}}{\left(50 \times 10^3 \cancel{\text{lbm/hr}} \right) \left(650.4 \cancel{\text{BTU/lbm}} \right) \left(2.93 \times 10^{-7} \cancel{\text{MWt-hr/BTU}} \right)} = 0.49 \quad (1.23)$$

Estimating the slip in the same manner (graphical C_o estimate)

[[(1.24)

(1.25)

]] The void fraction given by this power-to-flow ratio is very high; in fact, it is likely higher than what would commonly be encountered in normal service, where the bundle operating state would be constrained by the Operating Limit MCPR (OLMCPR). Stated a different way, in order to achieve [[]], this test bundle's MCPR could have violated the OLMCPR that would limit peak bundle power for an operating reactor. Reference [2] presents the detailed critical power data for ATLAS Test Assembly 751 (ATA751), which was used for both critical power and pressure drop testing. The critical power data for ATA751, peaking patterns B through I indicates that the critical power is very close to [[

]]

A.3. Application to Reactor Simulation

In general, thermal limits restrict the maximum achievable bundle power in any given core, at any given steady state operating condition. For a given set of thermal-hydraulic conditions, the OLMCPR directly limits the peak power bundle. The LHGR limit applies locally (on a rod and axial node basis) and indirectly limits bundle power by restricting the total peaking (i.e., LHGR effectively limits the allowable the combinations of axial power shapes and radial peaking patterns). As discussed in Section A.2.2, off-rated limits impose additional margin relative to limits applied at rated conditions. Limits developed to comply with ARTS¹⁴ take the most limiting of several parameters, including a flow dependent MCPR (i.e., $MCPR_F$), in order to constrain off-rated operation. An example of $MCPR_F$ is shown in Figure A-1.

¹³ Many BWRs operate with an OLMCPR around 1.40. Depending on system capabilities, lower OLMCPR values can be achieved and are encountered within the BWR fleet. However, the low flow conditions as discussed here would likely require off-rated limits corrections and additional margin, which would increase the effective OLMCPR.

¹⁴ Average Power Range Monitor, Rod Block Monitor, and Technical Specification (ARTS) improvement programs.

[[

]]

Figure A-1. Generic $MCPR_F$

A.3.1. Expected Void Fraction Ranges for Peak Bundles

The Findlay-Dix correlation can be applied to steady state critical power data in order to examine the expected maximum (exit) void fraction values for 10x10 bundles. Figure A-2 shows channel exit void fraction values predicted using the Findlay-Dix correlation¹⁵ for a set of GNF2 critical power data points. Note that the GNF2 design generally demonstrates higher critical power capability than GE14. Also, the data is for an inlet peaked APS, which maximizes critical power relative to other axial power distributions (e.g., outlet peaked). Only the [[

]]

The predicted exit void fractions extend to about [[]] at very low flow conditions. For bundle power-to-flow ratios less than about 13 MWt/Mlbm/hr-ft² (or mass fluxes greater than 0.8 Mlbm/hr-ft²), the highest exit void fractions at critical power are about [[]]. The onset of Boiling Transition (i.e., "BT" or film dryout) in BWR fuel bundles will occur on a rod (or rods) while other rods remain wetted; liquid inventory will also be available on unheated surfaces (e.g., channel walls) and in the form of droplets entrained in the vapor, so under forced

¹⁵ The correlation is applied with steam properties evaluated at 1,000 psia, i.e., not the "hand calculation" method presented in Sections A.2.1 and A.2.2. Also, the calculated void fractions are referenced to the fully rodDED bundle flow area, which slightly over estimates the exit void fraction values.

convective conditions, dryout does not correspond to $\alpha = 1.0$. For increasing power or heat flux, annular flow will eventually transition to mist flow (post dryout), where significant energy addition may be required to vaporize the remaining liquid.

[[

]]

Figure A-2. Predicted Exit Void Fractions Based on Critical Power Data

In Figure A-2, the points marked "Exit Void at MCPR = 1.4" are predicted at the same conditions as the critical power points, only constrained by a MCPR limit. The resulting power levels are reduced relative to critical power and more typical of operation. The reduced power is obtained using the definition of the bundle critical power ratio

$$MCPR = \frac{\text{Critical Power}}{\text{Power}} \quad (1.26)$$

Also, the generic $MCPR_F$ limit shown in Figure A-1 has been applied, using the approximation that 100% core flow corresponds to 1.0 Mlbm/hr-ft² bundle flow, 50% core flow corresponds to 0.5 Mlbm/hr-ft² bundle flow, etc., etc. Applying $MCPR_F$ (using the 102.5% curve) affects the low flow points (e.g., 0.3 Mlbm/hr-ft²). The reduced bundle power level becomes

$$\text{Power} = \frac{\text{Critical Power}}{MCPR} = \frac{\text{Critical Power}}{\max(1.4, MCPR_F)} \quad (1.27)$$

NEDO-33173, Supplement 1
Non-proprietary Version

As a point of reference, applying the limit $MCPR = 1.4$ for this bundle design and APS gives a peak bundle power of about [] at 0.8 Mlbm/hr-ft^2 and 20 Btu/lbm subcooling. This corresponds to a bundle power-to-flow ratio of about $9 \text{ MWt/Mlbm/hr-ft}^2$ and an exit void fraction of slightly less than 92%, as shown in the figure.

This exercise demonstrates that under steady state conditions typical of plant operation, expected values for 10×10 peak bundle maximum (exit) void fraction values are well within the application range of the Findlay-Dix correlation, as well as consistent with the predicted void range for the $10 \times 10 \Delta P$ data. The range of void fractions in the Findlay-Dix rod data covers from []

]] It is also worth noting that this discussion is presented in terms of the limiting power envelope represented by bundle critical power data, which is determined from tests, independent of the core operating domain. In other words, the void fraction information presented in this section is derived independent of the explicit core operating state (i.e., relative to a particular core or point on a power-flow map). Thermal limits information combined with bundle power-flow and subcooling information are sufficient for drawing conclusions regarding maximum expected (bundle exit) void fractions applicable to all operating domains.

A.3.2. Planar Average Versus Local (Subchannel) Void Fractions

In reactor simulation, the void correlation is applied to fuel channels to determine the one-dimensional void fraction (i.e., the planar average void fraction as a function of elevation). The void fraction information is essentially used to “look up” cross section data based on infinite lattice calculations, which are typically performed based on a single void value. This common technique used in core simulators ignores radial void fraction variations within bundles (which would be expected to be induced by variation in rod-to-rod local peaking). Studies have been conducted to examine this effect [13], [14]. Ama’s results [14] are well described and illustrate that radial void drift is expected to have a slight flattening effect on the pin power distribution due to local feedback. The simplified lattice physics treatment discussed here slightly overestimates the peak pin power.

APPENDIX B. "Method B" Pressure Drop

Table B-1 provides a summary of the expressions used to evaluate the pressure drop in a fuel bundle. The expressions are [[]]

Table B-1. Expressions Applied to Calculate the In-Channel Pressure Drop

Pressure Drop Term	Expression
Elevation	See Equation (4.9)
Friction	$\Delta P_{Frict} = f \left(\frac{\Delta z}{D_H} \right) \frac{\dot{m}^2}{2g_c \rho_{liq} A^2} \phi_{lo}^2$ <p>The single-phase friction factor (f) is based on a fit to the Moody curves, which are fit to Re, D_H, and surface roughness. [[The two-phase friction multiplier is the Chisolm multiplier (modified by Torbeck), which is a function of flow quality</p> $\phi_{lo}^2 = 1 + (\gamma' - 1) [X + \beta X(1 - X)]$ <p>where</p> <p style="text-align: center;">[[]]</p>
Local losses (spacers)	$\Delta P_{Loc} = \left(\frac{k}{A^2} \right) \frac{\dot{m}^2}{2g_c \rho_{liq}} \phi_{TPL}^2$ <p>The two-phase local loss multiplier [[]]</p>

NEDO-33173, Supplement 1
Non-proprietary Version

Pressure Drop Term	Expression
Acceleration	$\Delta P_{acc} = \frac{\dot{m}^2}{g_c A^2} \left[\frac{1}{\rho_{out}} - \frac{1}{\rho_{in}} \right]$ <p>where the “out” and “in” densities are [[</p> <p style="text-align: right;">]]</p>
Acceleration due to a flow area change	<p style="text-align: center;">[[</p> <p style="text-align: right;">]]</p>

APPENDIX C. ATLAS Measurement Uncertainties

Reference [2] contains a discussion of measurement uncertainties (basic measurement accuracies) for the ATLAS facility. The basic uncertainties are given in Table C-1.

Table C-1. Measurement Uncertainties [2]

Uncertainty Component	Value
Power (W)	[[
Mass Flow Rate (M)	
Inlet Subcooling (h)	
System Pressure (P)	
Differential Pressure (DP)]]

The system pressure uncertainty will affect the quality in the channel, which affects the two-phase ΔP . Similarly, the temperature uncertainty affects the inlet subcooling and the boiling length in the channel, which affects the two-phase ΔP . The mass flow rate uncertainty can be significant, as pressure drop generally varies with the square of the flow rate. The uncertainty associated with the power supply is neglected in this evaluation to ensure that the total error is underestimated. The total measurement uncertainty is a sum of the components in Table C-1.

$$\sigma_{Meas}^2 = \sigma_M^2 + \sigma_h^2 + \sigma_P^2 + \sigma_{DP}^2 + \cancel{\sigma_W^2} \quad (3.1)$$

An estimate of the mass flow rate sensitivity can be obtained from Figure 5-2, which shows the slope of measured ΔP versus mass flow rate for a series of tests. The family of curves in the figure shows that the slope increases with power due to higher two-phase pressure drops. Estimating the sensitivity based on relatively low power should underestimate the measurement uncertainty, which should (conservatively) overestimate the void uncertainty. [[

(3.2)

(3.3)

]]

The impact of inlet subcooling variation on the measurements is a little more difficult to evaluate. However, estimating the error impact as a change in flow quality allows an equivalent power change to be determined, which can be related to pressure drop through Figure 5-2 (consistent with the estimate for the flow rate error). Considering a one-dimensional, steady state mass and energy balance gives an expression for (exit) flow quality (see APPENDIX A)

$$X = \frac{\Delta h_{Sub}}{h_{fg}} + \frac{\dot{Q}}{\dot{m}h_{fg}} \quad (3.4)$$

An equivalent quality change for a given subcooling change (constant power) can be written

$$\Delta X = \frac{\Delta h_{Sub,1} - \Delta h_{Sub,2}}{h_{fg}} = \frac{\sigma_h}{h_{fg}} \quad (3.5)$$

The resulting quality change can be expressed as an equivalent power change (constant subcooling)

$$\Delta X = \frac{\Delta \dot{Q}}{\dot{m}h_{fg}} \quad (3.6)$$

[[

(3.7)

(3.8)

(3.9)

(3.10)

(3.11)

(3.12)

(3.13)

]]

This is an interesting result, in that the magnitude of the measurement uncertainty is relatively small in comparison to the measured pressure drop values [[
]], but worth consideration relative to the prediction error.

REFERENCES

- [1] NEDC-33238P, *GE14 Pressure Drop Characteristics*, eDRF Section 0000-0048-8535, December 2005.
- [2] NEDC-32874P, *Critical Power and Pressure Drop Tests of Simulated 10x10 Bundle Designs Applicable to GE14*,” March 2000.
- [3] Not Used
- [4] Not Used
- [5] Not Used
- [6] Not Used
- [7] John Mandel, *The Statistical Analysis of Experimental Data*, Dover Publications, Inc., New York, 1964.
- [8] Meyer, McClintock, Silvestri, and Spencer, *ASME Steam Tables*, The American Society of Mechanical Engineers, New York, 5th Edition, 1983.
- [9] R.T. Lahey and F.J. Moody, *The Thermal-Hydraulics of a Boiling Water Nuclear Reactor*, American Nuclear Society Monograph, 1984.
- [10] Paul Coddington and Rafael Macian, “A Study of the Performance of Void Fraction Correlations Used in the Context of Drift-Flux Two-Phase Flow Models,” *Nuclear Engineering and Design*, Vol. 215, No. 3, pp. 199-216 (June 2002).
- [11] Not Used.
- [12] Not Used.
- [13] NEDC-32601P-A, *Methodology and Uncertainties for Safety Limit MCPR Evaluations*, August 1999, Attachment A, “BWR Fuel Void Fraction.”
- [14] Tsuyoshi Ama, Hideaki Hyoudou, and Toshikazu Takeda, “Effect of Radial Void Distribution Within Fuel Assembly on Assembly Neutronic Characteristics,” *Journal of Nuclear Science and Technology*, Vol. 39, No. 1, pp. 90-100 (January 2002).

ENCLOSURE 3

MFN 07-478

Affidavit

GE-Hitachi Nuclear Energy Americas
AFFIDAVIT

I, Richard E. Kingston, state as follows:

- (1) I am Project Manager, Regulatory Affairs, GE-Hitachi Nuclear Energy (“GEH”), have been delegated the function of reviewing the information described in paragraph (2) which is sought to be withheld, and have been authorized to apply for its withholding.
- (2) The information sought to be withheld is contained in GE Licensing Topical Report, NEDC-33173P, Supplement 1, *Void Fraction Error Based on 10x10 Fuel Pressure Drop Data*, Class III (Proprietary Information), Revision 0, August 2007. The proprietary information in NEDC-33173P, Supplement 1, Revision 0, is identified by a single [[dotted underline inside double square brackets⁽³⁾]]. In each case, the superscript notation ⁽³⁾ refers to Paragraph (3) of this affidavit, which provides the basis for the proprietary determination.
- (3) In making this application for withholding of proprietary information of which it is the owner or licensee, GEH relies upon the exemption from disclosure set forth in the Freedom of Information Act (“FOIA”), 5 USC Sec. 552(b)(4), and the Trade Secrets Act, 18 USC Sec. 1905, and NRC regulations 10 CFR 9.17(a)(4), and 2.390(a)(4) for “trade secrets” (Exemption 4). The material for which exemption from disclosure is here sought also qualify under the narrower definition of “trade secret”, within the meanings assigned to those terms for purposes of FOIA Exemption 4 in, respectively, Critical Mass Energy Project v. Nuclear Regulatory Commission, 975F2d871 (DC Cir. 1992), and Public Citizen Health Research Group v. FDA, 704F2d1280 (DC Cir. 1983).
- (4) Some examples of categories of information which fit into the definition of proprietary information are:
 - a. Information that discloses a process, method, or apparatus, including supporting data and analyses, where prevention of its use by GEH's competitors without license from GEH constitutes a competitive economic advantage over other companies;
 - b. Information which, if used by a competitor, would reduce his expenditure of resources or improve his competitive position in the design, manufacture, shipment, installation, assurance of quality, or licensing of a similar product;
 - c. Information which reveals aspects of past, present, or future GEH customer-funded development plans and programs, resulting in potential products to GEH;

- d. Information which discloses patentable subject matter for which it may be desirable to obtain patent protection.

The information sought to be withheld is considered to be proprietary for the reasons set forth in paragraphs (4)a. and (4)b. above.

- (5) To address 10 CFR 2.390 (b) (4), the information sought to be withheld is being submitted to NRC in confidence. The information is of a sort customarily held in confidence by GEH, and is in fact so held. The information sought to be withheld has, to the best of my knowledge and belief, consistently been held in confidence by GEH, no public disclosure has been made, and it is not available in public sources. All disclosures to third parties including any required transmittals to NRC, have been made, or must be made, pursuant to regulatory provisions or proprietary agreements which provide for maintenance of the information in confidence. Its initial designation as proprietary information, and the subsequent steps taken to prevent its unauthorized disclosure, are as set forth in paragraphs (6) and (7) following.
- (6) Initial approval of proprietary treatment of a document is made by the manager of the originating component, the person most likely to be acquainted with the value and sensitivity of the information in relation to industry knowledge, or subject to the terms under which it was licensed to GEH. Access to such documents within GEH is limited on a "need to know" basis.
- (7) The procedure for approval of external release of such a document typically requires review by the staff manager, project manager, principal scientist or other equivalent authority, by the manager of the cognizant marketing function (or his delegate), and by the Legal Operation, for technical content, competitive effect, and determination of the accuracy of the proprietary designation. Disclosures outside GEH are limited to regulatory bodies, customers, and potential customers, and their agents, suppliers, and licensees, and others with a legitimate need for the information, and then only in accordance with appropriate regulatory provisions or proprietary agreements.
- (8) The information identified in paragraph (2) is classified as proprietary because it contains details of GEH's fuel design and licensing methodology.

The development of the methods used in these analyses, along with the testing, development and approval of the supporting methodology was achieved at a significant cost, on the order of several million dollars, to GEH or its licensor.

- (9) Public disclosure of the information sought to be withheld is likely to cause substantial harm to GEH's competitive position and foreclose or reduce the availability of profit-making opportunities. The information is part of GEH's comprehensive BWR safety and technology base, and its commercial value extends beyond the original development cost. The value of the technology base goes beyond the extensive physical database and analytical methodology and includes development of the expertise to determine and apply the appropriate evaluation process. In addition, the technology base includes the value derived from providing analyses done with NRC-approved methods.

The research, development, engineering, analytical, and NRC review costs comprise a substantial investment of time and money by GEH.


The precise value of the expertise to devise an evaluation process and apply the correct analytical methodology is difficult to quantify, but it clearly is substantial.

GEH's competitive advantage will be lost if its competitors are able to use the results of the GEH experience to normalize or verify their own process or if they are able to claim an equivalent understanding by demonstrating that they can arrive at the same or similar conclusions.

The value of this information to GEH would be lost if the information were disclosed to the public. Making such information available to competitors without their having been required to undertake a similar expenditure of resources would unfairly provide competitors with a windfall, and deprive GEH of the opportunity to exercise its competitive advantage to seek an adequate return on its large investment in developing and obtaining these very valuable analytical tools.

I declare under penalty of perjury that the foregoing affidavit and the matters stated therein are true and correct to the best of my knowledge, information, and belief.

Executed this 30th day of August 2007.


Richard E. Kingston
Project Manager, Regulatory Affairs
GE-Hitachi